JCBFM

Journal of Cerebral Blood Flow & Metabolism
2022, Vol. 42(4) 686–693

DOI: 10.1177/0271678X211062274
journals.sagepub.com/home/jcbfm

Arterial spin labeling demonstrates preserved regional cerebral blood flow in the P301L mouse model of tauopathy

Diana Kindler[1], Cinzia Maschio[2,3], Ruiqing Ni[1,2,3], Valerio Zerbi[3,4], Daniel Razansky[1,3,5] and Jan Klohs[1,3]

Abstract

There is growing evidence for the vascular contribution to cognitive impairment and dementia in Alzheimer's disease (AD) and other neurodegenerative diseases. While perfusion deficits have been observed in patients with Alzheimer's disease and tauopaties, little is known about the role of tau in vascular dysfunction. In the present study, regional cerebral blood (rCBF) was characterized in P301L mice with arterial spin labeling. No differences in rCBF in P301L mice compared to their age-matched non-transgenic littermates at mid (10–12 months of age) and advanced (19–21 months of age) disease stages. This was concomitant with preservation of cortical brain structure as assessed with structural T_2-weighted magnetic resonance imaging. These results show that hypoperfusion and neurodegeneration are not a phenotype of P301L mice. More studies are thus needed to understand the relationship of tau, neurodegeneration and vascular dysfunction and its modulators in AD and primary tauopathies.

Keywords

Arterial spin labeling, cerebral blood flow, tau, P301L, mouse models

Received 7 May 2021; Revised 13 October 2021; Accepted 20 October 2021

Introduction

There is growing evidence for the vascular contribution to cognitive impairment and dementia in Alzheimer's disease (AD) and other neurodegenerative diseases.[1,2] While effects of β-amyloid on vascular function have been well characterized,[3] little is known about the corresponding role of tau. Neuropathological studies have shown accumulation of tau oligomers in cerebral blood vessels of patients with AD but also in patients with primary tauopathies that do not have β-amyloid pathology.[4–6] Functional neuroimaging studies have demonstrated reductions in regional cerebral blood flow (rCBF) in patients with frontotemporal dementia (FTD).[7–12] The perfusion deficit has been shown to correlate with the degree of behavioral disturbances in FTD patients.[10] Furthermore, hypoperfusion has been found to occur presymptomatically in carriers of microtubule-associated protein tau (MAPT) and progranulin, which cause an autosomal dominant form of FTD,[13] raising the possibility that hypoperfusion is an early pathogenic contributor to the disease process. However, the cellular and molecular relationship between tau deposition, vascular dysfunction and neurodegeneration is not well understood. In this regard, investigations in animal models that display tau pathology may be useful.[14]

A variety of transgenic mouse lines with expression of several MAPT mutations such as N279K, ΔK280, P301L, P301S, v337 or R406 have been developed.[15–21]

[1]Institute for Biomedical Engineering, University of Zurich and ETH Zurich, Zurich, Switzerland
[2]Institute for Regenerative Medicine, University of Zurich, Zurich, Switzerland
[3]Zurich Neuroscience Center (ZNZ), Zurich, Switzerland
[4]Neural Control of Movement Lab, Department of Health Sciences and Technology, ETH Zurich, Zurich, Switzerland
[5]Institute of Pharmacology and Toxicology, University of Zurich, Zurich, Switzerland

Corresponding author:
Jan Klohs, Institute for Biomedical Engineering, ETH & University of Zurich, Vladimir-Prelog-Weg 4, 8093 Zurich, Switzerland.
Email: klohs@biomed.ee.ethz.ch

The mouse strains show pre-tangle formation and hyperphosphorylation of tau and aggregation of neurofibrillary tangles as well as neuroinflammation, cell dysfunction and neuronal loss; though the onset and severity of the phenotype varies among the different strains. To this end, vascular function has not been thoroughly studied in tauopathy models. Reports have shown vascular abnormalities such as perivascular accumulation of tau, changes in vessel morphology, impairment of blood-brain barrier integrity, and calcifications in the brain.[22–24] Studies assessing cerebral perfusion in models of FTD with arterial spin labeling (ASL) have yielded controversial results.[25–29] Here we characterized cerebral perfusion in P301L mice[30] with pulsed ASL. We asked the questions: (1) whether P301L mice show a hypoperfusion as a phenotype, and (2) if this is related to the disease stage.

Materials and methods

Animal model

Transgenic B6.Dg-Tg(Thy1.2-TauP301L)183Nitsch (P301L) mice have been engineered to express the human 4 repeat tau isoform under control of the murine Thy 1.2 promoter.[15] After generation, mice were backcrossed with C57BL/6J mice for >20 generations and maintained on a C57BL/6J background. All mice were maintained under specific pathogen-free conditions. Animals were housed in ventilated cages inside a temperature-controlled room (22°C, 50% air humidity), under a 12-hour dark/light cycle. Each cage housed up to five mice. Paper tissue and red Tecniplast mouse house® (Tecniplast, Milan, Italy) shelters were placed in cages as environmental enrichments. Cages and pelleted chow (3437PXL15, CARGILL) were steam-pressure sterilized. Water was acidified (pH 2.5–3.0). Both food and water were provided ad libitum.

All experiments were performed in accordance with the Swiss Federal Act on Animal Protection and were approved by the Cantonal Veterinary Office Zurich (permit number: ZH044/19). All animal experiments are reported in compliance with the ARRIVE guidelines 2.0.[31] A total of 9 hemizygous P301L and 10 non-transgenic littermates of 10-12-months of age (i.e. mid disease stage), and 16 hemizygous P301L mice and 13 non-transgenic littermates of 19-21-months of age (i.e. advanced disease stage) were used. From previous studies, we estimated variances in rCBF values from ASL measurements.[32,33] A sample size of $n = 3$ was calculated a priory for the primary end point rCBF, Wilcoxon-Mann-Whitney test with 2 groups to detect an estimated effect size of $f = 3.25$ (corresponding to 10% differences in rCBF values) with $\alpha = 0.05$ and $\beta = 0.2$.

Magnetic resonance imaging protocol

Magnetic resonance imaging (MRI) data was collected on a 7/16 small animal MR scanner (Pharmascan, Bruker Biospin GmbH, Ettlingen, Germany), equipped with an actively shielded gradient set of 760 mT/m with an 80 μs rise time and operated by a Paravision 6.0 software platform (Bruker Biospin GmbH). A circular polarized volume resonator was used for signal transmission and an actively decoupled mouse brain quadrature surface coil with integrated combiner and preamplifier for signal reception (Bruker BioSpin GmbH). Mice were anesthetized with an initial dose of 4% isoflurane (Abbott, Cham, Switzerland) in oxygen/air (200:800 ml/min) mixture and anesthesia were maintained with 1.5% isoflurane in oxygen/air mixture (100:400 ml/min), supplied via a nose cone. Mice were placed in prone position in the MRI scanner. Body temperature was monitored with a rectal temperature probe and kept within 36.5 ± 0.5°C. T_2-weighted anatomical reference images were acquired in coronal and sagittal orientations and served for accurate positioning of the arterial spin labeling (ASL) slice. A spin-echo sequence was used for positioning of the ASL slice with rapid acquisition relaxation enhancement (RARE) sequence. Five contiguous sagittal slices were acquired with a slice thickness = 1 mm; field-of-view = 20 × 20 mm; image matrix = 256 × 256; spatial resolution = 78 μm × 78 μm, echo time = 60 ms, relaxation time = 1700 ms, RARE factor = 8, and 2 averages.

For pulsed ASL, a flow-sensitive alternating inversion recovery (FAIR) sequence,[34] with a 2-shot segmented echo planar imaging (EPI) readout was implemented with the following parameters:[32,33] one axial slice, slice thickness = 1 mm, field-of-view = 20 × 20 mm; image matrix = 128 × 96, with a spatial resolution = 156 μm × 208 μm. Sixteen images with increasing inversion times (40, 100, 200, 300, 400, 500, 600, 800, 1000, 1200, 1500, 1800, 2100, 2400, 2700 and 3000 ms), inversion slab thickness = 4 mm, slice margin = 1.5 mm, echo time = 13 ms, recovery time = 10000 ms were obtained for the T_1 calculation. Inversion recovery data from the imaging slices was acquired after selective inversion interleaved with non-selective inversion. One slice was positioned on the midbrain to include the cortex and caudate putamen using the sagittal RARE image as a reference. A second slice was acquired more dorsal to include the thalamus. Fieldmap-based shimming was performed prior data acquisition using the automated MAPshim routine to improve the homogeneity of the magnetic field. To obtain structural information, a T_2-weighted spin-echo sequence was acquired with a RARE sequence for measurement of cortical thickness.

Two axial slices were acquired with a slice thickness = 1 mm; field-of-view = 20 × 20 mm; image matrix = 200 × 200; spatial resolution = 100 µm × 100 µm, echo time = 33 ms, relaxation time = 2500 ms, RARE factor = 8, and 2 averages. The total scan time per animal was approximately 30 min.

Image analysis and quantification

Maps of rCBF were generated by fitting the ASL images and T_1 maps in MATLAB R2019b (Mathworks, MA, USA).[34,35] The determination of selective T_1 and non-selective T_1 was performed by matching the mediated signal intensities in each voxel with a 3-parameter monoexponential T_1 relaxation curve. Furthermore, the residuals of both fits were assessed as the Euclidean distance between the actual data point and the T_1 curve fitted in each experiment. Image analysis was performed by a person blinded to the genotype of the animal. Region-of-interests (ROIs) were manually drawn using ImageJ (National Institute of Health, USA). A mouse brain atlas was used as anatomical reference.[36] ROIs were drawn over the left and right cortex, caudate putamen, and thalamus. Individual ROIs for each region were averaged. The cortical thickness was measured on the T_2-weighed axial images and values were averaged for each slice.

Immunofluorescence staining. Three P301L and three non-transgenic littermate mice were perfused under ketamine/xylazine/acepromazine maleate anesthesia (75/10/2 mg/kg body weight, i.p. bolus injection) with ice-cold 0.1 M PBS (pH 7.4) and in 4% paraformaldehyde in 0.1 M PBS (pH 7.4), and fixed for 24 h in 4% paraformaldehyde (pH 7.4) and then stored in 0.1 M PBS (pH 7.4) at 4°C. Coronal brain sections (40 µm) were cut around Bregma 0 to −2 mm and stained with anti-phosphorylated tau (pSer202/pThr205) antibody AT-8 (Invitrogen, MN1020, 1:1000). As 2nd we used antibody goat-anti-Rabbit Alexa488 (Invitrogen A11034, 1:200). Sections were counterstained using DAPI Sigma D9542-10MG, 1:1000, and mounted with VECTASHIELD fluorescent mounting media (Vector Laboratories H-1000-10). The brain sections were imaged at ×20 magnification using Axio Oberver Z1 slide scanner (Zeiss, Germany) using the same acquisition setting for all brain slices and magnification and using a Leica SP8 confocal microscope (Leica, Germany). The images were analyzed by a person blinded to the genotype using Qupath and ImageJ (NIH, U.S.A).

Statistical analysis. Data are presented as mean ± SD. Statistical testing was performed using SigmaStat 13 (Systat Software Inc) and GraphPad Prism 9 (GraphPad). Gender differences across P301L and non-transgenic littermates were examined using a Fisher exact test. ROI data was tested using the Shapiro–Wilk test, which showed that not all data is normally distributed. Thus, Mann-Whitney Rank Sum tests were used to examine differences in rCBF, cortical thickness and area of AT8-antibody coverage between P301L and non-transgenic littermates at a given age level. The statistical significance level was set to $p < 0.05$.

Results

Animal characteristics

The animal characteristics for images analyzed are shown in Table 1. Post hoc, 5 of the 48 data sets were excluded due to health issues (3), or low data quality (2). The differences in the proportion of male and female mice was not different across the cohort of 10–12-months old animals ($n = 18$, $p = 1.0$) and 19–20-months old animals ($n = 25$, $p = 0.07$). There were no statistically significant differences between the ages of P301L mice and non-transgenic littermates for the 10–12-months-of-age cohort (P301L: 11.4 ± 0.2 vs non-transgenic littermates: 11.4 ± 0.2, $p = 1.0$) and 19–21-months of age cohort (P301L: 21.1 ± 0.6 vs non-transgenic littermates: 20.8 ± 0.5, $p = 175$).

Preserved rCBF and cortical structure in mid and advanced disease stage of tau pathology

We used P301L mice to investigate the effect of tau pathology on rCBF with ASL. Mice were studied at 10–12 and 19–21 months-of-age at which they show mid and advanced disease stage pathology such as tau deposition, calcifications and microstructural abnormalities.[15,24,37,38] Model fits were similar between animals of both groups (Supplementary Figure 1). At both disease stages, we did not detect significant differences in rCBF between P301L and non-transgenic littermates in the neocortex, caudate putamen and thalamus (Figure 1(a) and (c)). There were no statistically significant differences in rCBF values when comparing male and female mice of each group separately. Furthermore, we estimated cortical thickness on T_2-weighed structural MR images as a marker of

Table 1. Animal characteristics.

	Non-transgenic			P301L		
Age	Male	Female	Total	Male	Female	Total
10–12 months	3	7	10	3	5	8
19–21 months	7	3	10	4	11	15

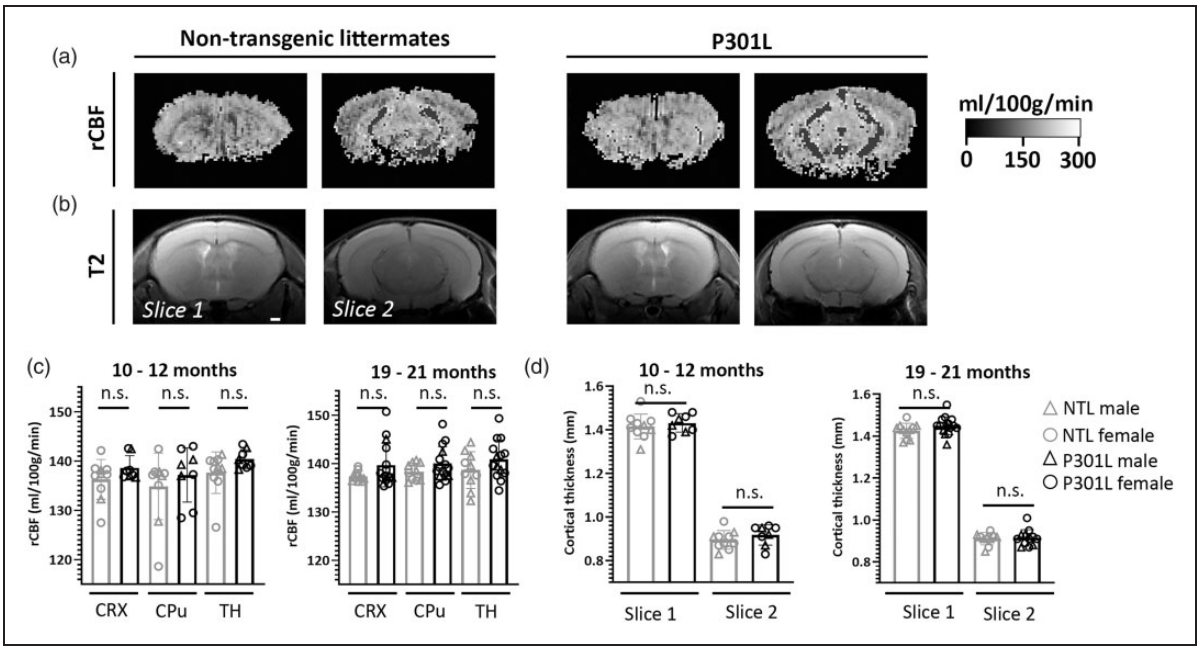

Figure 1. Preserved rCBF in the P301L mouse model of tauopathy a) rCBF maps derived from ASL measurements and b) axial T_2-weighted images for calculation of cortical thickness. c) ROI analysis of rCBF maps shows no differences in regional CBF in the neocortex (CRX), caudate putamen (CPu) and thalamus (TH) between 10–12-months and 19–21-months old male (grey triangle) and female (grey circle) non-transgenic littermates (NTL) compared to age-matched male (black triangle) and female (black circle) P301L mice. A Mann-Whitney Rank Sum test. d) No differences in cortical thickness between groups is observed. A Mann-Whitney Rank Sum test.

neurodegeneration. No statistical differences in cortical thickness between P301L mice and non-transgenic littermates were recognized for both age groups (Figure 1(b) and (d)). When comparing male and female mice of each group separately, there were also no statistically significant differences in cortical thickness between animals of the same gender and different genotypes.

Cerebral tau pathology

To verify the presence of tauopathy we prepared brain sections of P301L and non-transgenic littermates and performed immunofluorescence stainings with Alexa488-AT-8 antibody, which binds to sarkosyl-insoluble tau and soluble hyperphosphorylated tau,[39,40] and DAPI. Confocal imaging and quantification of tau coverage with a slide scanner in the hippocampus demonstrated tauopathy deposits in P301L mice at mid disease stage (Figure 2(a) and (b)). No tau deposits were observed in non-transgenic littermates.

Discussion

Different transgenic tauopathy mouse lines based on MAPT mutations have been developed.[15–21] While these lines commonly display tau accumulation, neuroinflammation and neuronal loss, ASL studies assessing cerebral perfusion in these models have yielded inconsistent results. Studies by Wells et al. (2015) and Homes et al. (2016) did not find differences in 7-months and 7.5-months old rTG4510 mice compared to age-matched non-transgenic littermates respectively,[25,29] whilst an ASL study by Park et al. (2020) has reported normal rCBF values in rTG4510 mice at 2–3 months of age.[27] Govaerts et al. (2019) found in a longitudinal study rCBF values to be similar in 3, 6 and 12 months-old Tau.P301L mice compared to non-transgenic littermates.[28] In a bigenic mouse model that was generated from the Tau.P301L strain and that displayed also β-amyloid pathology in addition to tau pathology, had reductions in rCBF.[28] This demonstrates relation of β-amyloid deposition with hypoperfusion that have also been found in mouse models of cerebral amyloidosis.[32,33,41–43] In contrast, a study by Holmes found elevated cortical but normal thalamic rCBF in 7.5-months old rTG4510 mice.[29] Wells et al. (2015) has revealed hyperperfusion in cortical, hippocampal and thalamic brain regions in 8.5–9.5 months old rTG4510 mice.[26] A cortical hypoperfusion was recently reported by Park et al. (2020) in 2–3 months old PS19 mice.[27] In the current study, we observed a preserved perfusion in P301L mice at mid (i.e. 10–12-months of age) and advanced (i.e. 19–21-months of

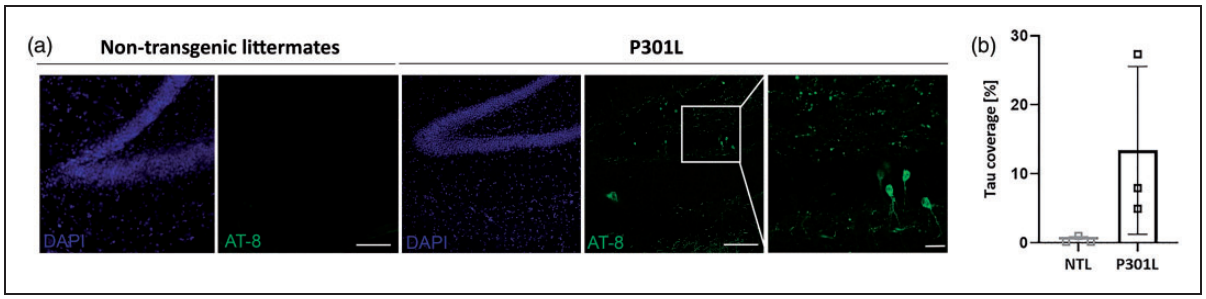

Figure 2. Tauopathy in the P301L mouse. a) Immunofluorescence stainings of brain sections of non-transgenic littermates and P301L mice with Alexa488-AT-8 antibody (green) and DAPI (blue). Confocal images of the hippocampus demonstrated tau deposits in P301L mice at mid disease stage that were not observed in non-transgenic littermates. Scale bar = 100 μm and 20 μm for the zoom-ins. b) Quantification of the mean area covered by the AT-8 antibody staining (tau coverage) in NTL (n = 3) and P301L (n = 3) mice. Mann-Whitney Rank Sum test, *$p < 0.05$.

age) stage of tau pathology compared to their age-matched non-transgenic littermates. This was concomitant with no visible cortical atrophy.

Variations in the perfusion phenotype of different transgenic mouse models of tauopathy may arise due to a number of factors. Important ones are the type of tau mutation, promoter of transgene expression used and zygosity, all determining the transgene expression levels and cellular localization and thus the phenotype severity. Moreover, previous studies using ASL in mouse models of tauopathy have assessed cohorts of mice of different ages, that translate in different disease stages. In the rTG4510 mouse line transgenic tau P301L expression is driven by a Ca^{2+}/calmodulin kinase II promoter and displays a pronounced loss of neurons, rapidly progressing between 2-7 months of age.[16,17] Tau.P301L express the P301L mutation under the Thy1 promoter,[44] while the P301L mice used in our study express the P301L mutation under the Thy 1.2 promoter,[15] exhibiting early tau accumulation and neuronal cell death.[15,44] However, T_2-weighed structural MR images revealed that no cerebral atrophy in P301L mice, even at an advanced disease stage. PS19 mice have the P301S mutation expressed under the mouse prion protein promoter and display neuronal loss at 9-12 months of age.[21] Hence, the observed changes in rCBF do not seem to be related to the severity of neurodegeneration in these models. A study in FTD patients has shown a regional discordance between atrophy and perfusion deficits.[7–9,12] Furthermore, hypoperfusion is not deemed to be linked to the cortical tau accumulation as in PS19 mice hypoperfusion occurred at an age where tau is phosphorylated, but without the formation of neurofibrillary tangles,[27] whereas in rTG4510, Tau.P301L and P301L mice the rCBF was preserved in the presence of strong tau accumulation. This may point to a role of tau oligomers that have the ability to translocate across the brain and which have also been found in the vessels and perivascular spaces.[4–6,22] However, the exact role of the species in vascular function has not been elucidated. Moreover, as patients with the same MAPT mutation can show distinct phenotypes,[45] a different genetic modifier might play a role. Thus, the genetic background of the strains or the transgene insertion may account for differences in the perfusion phenotype.[46]

Another important modulating factor for the disease phenotype is gender. In AD there is not only a higher prevalence of the disease in women as compared to men,[47,48] but it is also associated with a higher tau cerebrospinal fluid level, cortical tau load and degree of neurodegeneration (Filon et al., 2016; Hohman et al., 2018).[49–51] Sexual dimorphism of the behavioral and neuropathological phenotype in animal models of tauopathy have been reported, but yielded mixed results. In both studies by Wells et al. (2015) and Holmes et al. (2016) rCBF was assessed in female rTg4510 mice.[25,26,29] It has been reported that female rTG4510 mice display higher levels of hyperphosphorylated tau associated with more severe impairment in spatial learning and memory than male mice,[52] that have been used in the ASL study by Park et al. (2020).[27] In contrast, P301S showed a stronger cognitive deficit and neuropathology in male transgenic mice,[53] that have been used in the perfusion study by Park et al. (2020).[27] Gender differences in P301L mice have so far not been reported. In a recent study, we have seen no differences in the number of cerebral calcifications between male and female P301L mice and have thus used mice of both gender. Statistical analysis has not identified any gender-related effects on the rCBF values and cortical atrophy.

In addition, methodological differences in rCBF assessment may play a role to explain differences between studies, with the choice of anesthesia being very important in this regard. Isoflurane, that is commonly used in mouse ASL studies and that we have

used in the current study, is a vasodilator, affects peripheral hemodynamics and can impair cerebral autoregulation in a dose-dependent fashion.[54–56] Different concentrations of isoflurane have been used in breathing gases in ASL studies of tauopathy model. Even when similar concentrations of the anesthetic are used, differences in the delivery systems (flow rates of carrier gases, tubing, potential accumulation in MRI supports etc.) between labs will result in slightly different concentrations of isoflurane transmitted to the animal and hampers a precise comparison of results. We have assessed rCBF using 1.5% isoflurane, at a concentration where we previously detected differences in rCBF and vascular reactivity in the arcAβ mouse model of cerebral amyloidosis.[32,33] However, as isoflurane at that concentration increases rCBF and serves as a vascular stimulus it may be a confounding factor in functional studies assessing rCBF in P301L mice. Holmes at al. (2016) has shown differences in measured rCBF values in 9-months old rTG4510 mice, where hyperperfusion was seen when 2% but not when 1.5% isoflurane were used. However, in two publications from Wells et al. (2015) increased rCBF in 8.5-months old rTG4510 mice was found when 1.5% isoflurane was used,[26] while no change in rCBF was seen in 7.5-months old rTG4510 mice when 2% isoflurane was used.[25] However, Govaert et al. (2018) used a ketamine/midazolam anesthesia, which is known to decrease rCBF,[57] and have not found differences in rCBF in Tau.P301L mice.[28]

Currently, the mechanisms underlying tau-related hemodynamic dysfunction are not well understood. Neuroimaging studies have shown the co-existence of hypoperfusion and hypometabolism in certain brain areas in patients with frontotemporal dementia and animal models, which may indicate a reduced neuronal activity/metabolic demand may underlie the observed hypoperfusion.[58,59] Several studies in mouse models of tauopathy have provided evidence for pathological alteration of the cerebral vasculature related to tau,[22–24] but, unlike to β-amyloid whose effects on vascular function and integrity have been largely shown,[32,33,41–43,60] the effect of tau deposition on hemodynamic dysfunction is largely unknown. Recent work by Park et al. (2020) demonstrated a tau-induced impairment of neurovascular coupling.[27] They showed that during glutamatergic synaptic activity there is tau-induced dissociation of neuronal nitric oxide synthase from postsynaptic density 95 and a reduced production of nitric oxide, which reduces the vasodilation of cerebral arterioles and thus reduces rCBF. However, more research is needed to elucidate the role of tau in AD and other tauopathies.

In summary, no differences in rCBF, as quantified with pulsed ASL, were identified in P301L mice at mid and advanced stage of tau pathology with no changes manifested also in their brain structure. These results indicate an absent phenotype in P301L mice, further suggesting that hypoperfusion and neurodegeneration are not related to accumulation of tau. More work is needed to understand the relationship of tau, neurodegeneration and vascular dysfunction and its modulators in AD and primary tauopathies.

Availability of data and materials

The data used and analyzed in the current study are available from the corresponding authors upon request.

Funding

The author(s) disclosed receipt of the following financial support for the research, authorship, and/or publication of this article: JK received funding from the Swiss National Science Foundation (320030_179277), the Olga Mayenfisch Stiftung, and the Vontobel foundation. DR acknowledges funding from the Swiss National Science Foundation (310030_192757).

Acknowledgement

The authors acknowledge Mark Augath (Institute for Biomedical Engineering), Vasil Kecheliev and Uwe Konietzko (Institute for Regenerative Medicine) for technical support.

Authors' contributions

JK conceived and designed the study. DK, CM, RN, VZ acquired and analyzed the data. RN, VZ, DR, JK interpreted the results. JK wrote the manuscript. All authors contributed to revising of the manuscript.

Declaration of conflicting interests

The author(s) declared no potential conflicts of interest with respect to the research, authorship, and/or publication of this article.

ORCID iDs

Ruiqing Ni https://orcid.org/0000-0002-0793-2113
Jan Klohs https://orcid.org/0000-0003-4065-2807

Supplemental material

Supplemental material for this article is available online.

References

1. Klohs J. An integrated view on vascular dysfunction in Alzheimer's disease. *Neurodegener Dis* 2019; 19: 109–127.
2. Zlokovic BV. Neurovascular pathways to neurodegeneration in Alzheimer' s disease and other disorders. *Nat Rev Neurosci* 2011; 12: 723–738.
3. Klohs J, Rudin M, Shimshek DR, et al. Imaging of cerebrovascular pathology in animal models of Alzheimer's disease. *Front Aging Neurosci* 2014; 6: 32.

4. Lasagna-Reeves CA, Castillo-Carranza DL, Sengupta U, et al. Identification of oligomers at early stages of tau aggregation in Alzheimer' s disease. *FASEB J* 2012; 26: 1946–1959. doi:10.1096/fj.11-199851.
5. Castillo-Carranza DL, Nilson AN, Van Skike CE, et al. Cerebral microvascular accumulation of tau oligomers in Alzheimer's disease and related tauopathies. *Aging Dis* 2017; 8: 257–266.
6. Merlini M, Wanner D and Nitsch RM. Tau pathology-dependent remodelling of cerebral arteries precedes Alzheimer's disease-related microvascular cerebral amyloid angiopathy. *Acta Neuropathol* 2016; 131: 737–752.
7. Steketee RME, Bron EE, Meijboom R, et al. Early-stage differentiation between presenile Alzheimer's disease and frontotemporal dementia using arterial spin labeling MRI. *Eur Radiol* 2016; 26: 244–253.
8. Shimizu S, Zhang Y, Laxamana J, et al. Concordance and discordance between brain perfusion and atrophy in frontotemporal dementia. *Brain Imaging Behav* 2010; 4: 46–54.
9. Zhang Y, Schuff N, Ching C, et al. Joint assessment of structural, perfusion, and diffusion MRI in Alzheimer's disease and frontotemporal dementia. *Int J Alzheimers Dis* 2011; 2011: 546871.
10. Hu WT, Wang Z, Lee VMY, et al. Distinct cerebral perfusion patterns in FTLD and AD. *Neurology* 2010; 75: 881–888.
11. Binnewijzend MAA, Kuijer JPA, Van Der Flier WM, et al. Distinct perfusion patterns in Alzheimer's disease, frontotemporal dementia and dementia with Lewy bodies. *Eur Radiol* 2014; 24: 2326–2333.
12. Du AT, Jahng GH, Hayasaka S, et al. Hypoperfusion in frontotemporal dementia and Alzheimer disease by arterial spin labeling MRI. *Neurology* 2006; 67: 1215–1220.
13. Dopper EGP, Chalos V, Ghariq E, et al. Cerebral blood flow in presymptomatic MAPT and GRN mutation carriers: a longitudinal arterial spin labeling study. *NeuroImage Clin* 2016; 12: 460–465.
14. Götz J and Ittner LM. Animal models of Alzheimer's disease and frontotemporal dementia. *Nat Rev Neurosci* 2008; 9: 532–544.
15. Götz J, Chen F, Van Dorpe J, et al. Formation of neurofibrillary tangles in P301L tau transgenic mice induced by Aβ42 fibrils. *Science* 2001; 293: 1491–1495.
16. Santacruz K, Lewis J, Spires T, et al. Medicine: Tau suppression in a neurodegenerative mouse model improves memory function. *Science* 2005; 309: 476–481.
17. Ramsden M, Kotilinek L, Forster C, et al. Age-dependent neurofibrillary tangle formation, neuron loss, and memory impairment in a mouse model of human tauopathy (P301L). *J Neurosci* 2005; 25: 10637–10647.
18. Tatebayashi Y, Miyasaka T, Chui DH, et al. Tau filament formation and associative memory deficit in aged mice expressing mutant (R406W) human tau. *Proc Natl Acad Sci USA* 2002; 99: 13896–13901.
19. Dawson HN, Cantillana V, Chen L, et al. The tau N279K exon 10 splicing mutation recapitulates frontotemporal dementia and parkinsonism linked to chromosome 17 tauopathy in a mouse model. *J Neurosci* 2007; 27: 9155–9168.
20. Mocanu MM, Nissen A, Eckermann K, et al. The potential for β-structure in the repeat domain of tau protein determines aggregation, synaptic decay, neuronal loss, and coassembly with endogenous tau in inducible mouse models of tauopathy. *J Neurosci* 2008; 28: 737–748.
21. Yoshiyama Y, Higuchi M, Zhang B, et al. Synapse loss and microglial activation precede tangles in a P301S tauopathy mouse model. *Neuron* 2007; 53: 337–351.
22. Blair LJ, Frauen HD, Zhang B, et al. Tau depletion prevents progressive blood-brain barrier damage in a mouse model of tauopathy. *Acta Neuropathol Commun* 2015; 3: 8.
23. Bennett RE, Robbins AB, Hu M, et al. Tau induces blood vessel abnormalities and angiogenesis-related gene expression in P301L transgenic mice and human Alzheimer's disease. *Proc Natl Acad Sci USA* 2018; 115: E1289–E1298.
24. Ni R, Zarb Y, Kuhn GA, et al. SWI and phase imaging reveal intracranial calcifications in the P301L mouse model of human tauopathy. *MAGMA* 2020; 33: 769–781.
25. Wells JA, Holmes HE, O'Callaghan JM, et al. Increased cerebral vascular reactivity in the tau expressing rTg4510 mouse: evidence against the role of tau pathology to impair vascular health in Alzheimer's disease. *J Cereb Blood Flow Metab* 2015; 35: 359–362.
26. Wells JA, O'Callaghan JM, Holmes HE, et al. In vivo imaging of tau pathology using multi-parametric quantitative MRI. *Neuroimage* 2015; 111: 369–378.
27. Park L, Hochrainer K, Hattori Y, et al. Tau induces PSD95–neuronal NOS uncoupling and neurovascular dysfunction independent of neurodegeneration. *Nat Neurosci* 2020; 23: 1079–1089.
28. Govaerts K, Lechat B, Struys T, et al. Longitudinal assessment of cerebral perfusion and vascular response to hypoventilation in a bigenic mouse model of Alzheimer's disease with amyloid and tau pathology. *NMR Biomed* 2019; 32: 1–12.
29. Holmes HE, Colgan N, Ismail O, et al. Imaging the accumulation and suppression of tau pathology using multiparametric MRI. *Neurobiol Aging* 2016; 39: 184–194.
30. Götz J, Chen F, Barmettler R, et al. Tau filament formation in transgenic mice expressing P301L tau. *J Biol Chem* 2001; 276: 529–534.
31. Percie N, Hurst V, Ahluwalia A, et al. The ARRIVE guidelines 2.0: updated guidelines for reporting animal research. *BMC Vet Res* 2020; 16: 242.
32. Ni R, Rudin M and Klohs J. Cortical hypoperfusion and reduced cerebral metabolic rate of oxygen in the arcAβ mouse model of Alzheimer's disease. *Photoacoustics* 2018; 10: 38–47.
33. Ni R, Kindler DR, Waag R, et al. FMRI reveals mitigation of cerebrovascular dysfunction by bradykinin receptors 1 and 2 inhibitor noscapine in a mouse model of cerebral amyloidosis. *Front Aging Neurosci* 2019; 10: 1–14.

34. Kim S, -G. Quantification of relative cerebral blood flow change by flow-sensitive alternating inversion recovery (FAIR) technique: Application to functional mapping. *Magn Reson Med* 1995; 34: 293–301.
35. Buxton RB, Frank LR, Wong EC, et al. A general kinetic model for quantitative perfusion imaging with arterial spin labeling. *Magn Reson Med* 1998; 40: 383–396.
36. Paxinos G and Franklin KBJ. *Paxinos and Franklin's the Mouse Brain in Stereotaxic Coordinates*. 4th Edn., Cambridge, MA: Academic Press. 2001.
37. Ni R, Chen Z, Gerez JA, et al. Detection of cerebral tauopathy in P301L mice using high-resolution large-field multifocal illumination fluorescence microscopy. *Biomed Opt Express* 2020; 11: 4989–5002.
38. Massalimova A, Ni R, Nitsch RM, et al. Research Article DTI reveals whole-brain microstructural changes in the P301L mouse model of tauopathy. 2020; 20: 173–184.
39. Goedert M, Jakes R and Vanmechelen E. Monoclonal antibody AT8 recognises tau protein phosphorylated at both serine 202 and threonine 205. *Neurosci Lett* 1995; 189: 167–170.
40. Delobel P, Lavenir I, Fraser G, et al. Analysis of tau phosphorylation and truncation in a mouse model of human tauopathy. *Am J Pathol* 2008; 172: 123–131.
41. Weidensteiner C, Metzger F, Bruns A, et al. Cortical hypoperfusion in the B6.PS2APP mouse model for Alzheimer's disease: comprehensive phenotyping of vascular and tissular parameters by MRI. *Magn Reson Med* 2009; 62: 35–45.
42. Massaad C. a, Amin SK, Hu L, et al. Mitochondrial superoxide contributes to blood flow and axonal transport deficits in the Tg2576 mouse model of Alzheimer's disease. *PLoS One* 2010; 5: e10561.
43. Faure a, Verret L, Bozon B, et al. Impaired neurogenesis, neuronal loss, and brain functional deficits in the APPxPS1-Ki mouse model of Alzheimer's disease. *Neurobiol Aging* 2011; 32: 407–418.
44. Terwel D, Lasrado R, Snauwaert J, et al. Changed conformation of mutant Tau-P301L underlies the moribund tauopathy, absent in progressive, nonlethal axonopathy of tau-4R/2N transgenic mice. *J Biol Chem* 2005; 280: 3963–3973.
45. Kobayashi T, Mori H, Okuma Y, et al. Contrasting genotypes of the tau gene in two phenotypically distinct patients with p301L mutation of frontotemporal dementia and parkinsonism linked to chromosome 17. *J Neurol* 2002; 249: 669–675.
46. Gamache J, Benzow K, Forster C, et al. Factors other than hTau overexpression that contribute to tauopathy-like phenotype in rTg4510 mice. *Nat Commun* 2019; 10: 2479.
47. Carter CL, Resnick EM, Mallampalli M, et al. Sex and gender differences in Alzheimer's disease: recommendations for future research. *J Womens Health (Larchmt)* 2012; 21: 1018–1023.
48. Plassman BL, Langa KM, Fisher GG, et al. Prevalence of dementia in the United States: the aging, demographics, and memory study. *Neuroepidemiology* 2007; 29: 125–132.
49. Filon JR, Intorcia AJ, Sue LI, et al. Gender differences in Alzheimer disease: brain atrophy, histopathology burden, and cognition. *J Neuropathol Exp Neurol* 2016; 75: 748–754.
50. Hohman TJ, Dumitrescu L, Barnes LL, et al.; Alzheimer's Disease Genetics Consortium and the Alzheimer's Disease Neuroimaging Initiative. Sex-specific association of apolipoprotein e with cerebrospinal fluid levels of tau. *JAMA Neurol* 2018; 75: 989–998.
51. Buckley RF, Mormino EC, Rabin JS, et al. Sex differences in the association of global amyloid and regional tau deposition measured by positron emission tomography in clinically normal older adults. *JAMA Neurol* 2019; 76: 542.
52. Yue M, Hanna A, Wilson J, et al. Sex difference in pathology and memory decline in rTg4510 mouse model of tauopathy. *Neurobiol Aging* 2011; 32: 590–603.
53. Sun Y, Guo Y, Feng X, et al. The behavioural and neuropathologic sexual dimorphism and absence of MIP-3α in tau P301S mouse model of Alzheimer's disease. *J Neuroinflammation* 2020; 17: 1–18.
54. Munting LP, Derieppe MPP, Suidgeest E, et al. Influence of different isoflurane anesthesia protocols on murine cerebral hemodynamics measured with pseudo-continuous arterial spin labeling. *NMR Biomed* 2019; 32: 1–12.
55. Hoffman WE, Edelman G, Kochs E, et al. Cerebral autoregulation in awake versus isoflurane-anesthetized rats. *Anesth Analg* 1991; 73: 753–757.
56. Strebel S, Lam A, Matta B, et al. Dynamic and static cerebral autoregulation during isoflurane, desflurane, and propofol anesthesia. *Anesthesiology* 1995; 83: 66–76.
57. Björkman S, Åkeson J, Nilsson F, et al. Ketamine and midazolam decrease cerebral blood flow and consequently their own rate of transport to the brain: an application of mass balance pharmacokinetics with a changing regional blood flow. *J Pharmacokinet Biopharm* 1992; 20: 637–652.
58. Verfaillie SCJ, Adriaanse SM, Binnewijzend MAA, et al. Cerebral perfusion and glucose metabolism in Alzheimer's disease and frontotemporal dementia: two sides of the same coin? *Eur Radiol* 2015; 25: 3050–3059.
59. Kleinberger G, Brendel M, Mracsko E, et al. The FTD-like syndrome causing TREM 2 T66M mutation impairs microglia function, brain perfusion, and glucose metabolism. *Embo J* 2017; 36: 1837–1853.
60. Klohs J, Rudin M, Shimshek DR, et al. Imaging of cerebrovascular pathology in animal models of Alzheimer's disease. *Front Aging Neurosci* 2014; 6: 1–30.